Interpolating between bumps and chimeras

Carlo R. Laing[1]
School of Natural and Computational Sciences, Massey University,
Private Bag 102-904 North Shore Mail Centre, Auckland,
New Zealand
c.r.laing@massey.ac.nz

(Dated: October 6, 2021)

A "bump" refers to a group of active neurons surrounded by quiescent ones while a "chimera" refers to a pattern in a network in which some oscillators are synchronized while the remainder are asynchronous. Both types of pattern have been studied intensively, but are sometimes conflated due to their similar appearance and existence in similar types of networks. Here we numerically study a hybrid system which linearly interpolates between a network of theta neurons which supports a bump at one extreme, and a network of phase oscillators which supports a chimera at the other extreme. Using the Ott/Antonsen ansatz we derive the equation describing the hybrid network in the limit of an infinite number of oscillators, and perform bifurcation analysis on this equation. We find that neither the bump nor chimera persist over the whole range of parameters, and the hybrid system shows a variety of other states such as spatiotemporal chaos, travelling waves, and modulated travelling waves.

Keywords: Bumps, Chimera states, Coupled oscillators, Bifurcations, Collective behavior in networks

"Bumps" are spatially-localised groups of firing neurons surrounded by quiescent neurons. Chimeras are patterns in coupled oscillator networks for which some oscillators are synchronised while others are asynchronous. These two types of pattern are visually similar but are created through different mechanisms. Here we study a hybrid model which in one extreme is a network of theta neurons which supports a bump state and in the other extreme is a network of Kuramoto phase oscillators which supports a chimera. We interpolate between these two extremes and find that neither the bump nor the chimera persist. Instead we find travelling waves, spatially uniform periodic states and spatiotemporal chaos, among other states.

I. INTRODUCTION

In the field of neuronal network modelling a "bump" refers to a spatially-localised region of active neurons, surrounded by quiescent neurons. They are often studied in models for head direction[1] and working memory[2,3], among others. Bumps occur in continuum neural field models[4–11] and also in networks of spiking neurons[12–15]. Networks supporting bumps are often bistable, with the "all-off" state, in which few or no neurons are firing, also being an attractor. It is this bistability that makes these networks candidates for memory units in which a scalar (the position of the bump) can be stored. Chimeras are a more recently discovered state, in which — for a one dimensional network of coupled oscillators — some of the oscillators form a contiguous group of synchronised oscillators, while the remainder are asynchronous[16–20]. They have gained a great deal of attention recently and have been observed in two[21,22] and three[23] spatial dimensions as well as in experiments[24,25]. Systems supporting chimeras are often bistable, with the fully synchronised state also being stable.

Bumps and chimeras are visually and conceptually similar, both occurring in networks of oscillators with nonlocal coupling[19]. This has lead to some authors conflating the two states[26], a situation probably exacerbated by the labelling of many states with coexisting synchrony and asynchrony as chimeras[27], as well as the study of chimeras in networks of model neurons[28–31]. However, the states are different: in networks supporting bumps the individual unit, typically a model neuron, undergoes a transition from quiescence to periodic firing as its input from others, often in the form of a current, is increased. Thus a bump in a network with "Mexican hat" coupling (positive for near neighbours and negative for more distant ones) consists of a region of active neurons whose activity keeps them and their close neighbours firing, while suppressing neurons further away. The quiescent neurons do not have enough input to fire and thus provide no input to the active neurons. Quiescent neurons have similar states (near the stable fixed point of an uncoupled neuron) but are not "synchronised" as they are not oscillating. Indeed, classical neural field models supporting

bumps involve only firing frequencies of neurons, with no information about their phases[4,32]. Conversely, in the networks in which chimeras were first found[16–18,20] the individual unit is an oscillator, freely running at a fixed frequency when uncoupled. A chimera occurs when the form of the coupling is such that a synchronised group of oscillators creates a "field" to which they can lock and thus remain synchronised but which is too weak for the asynchronous oscillators to lock to. The asynchronous oscillators contribute only weakly to the field. The difficulty in choosing the form of such a field and an appropriate type of oscillator means that many of the systems in which chimeras have been observed[28,33–39] are "close" to Kuramoto phase oscillator networks in which they were originally observed and analysed[16–19].

In this paper we consider a one-parameter "hybrid" model network which at one extreme is a network of theta neurons supporting a stable bump state, and at the other extreme is a network of Kuramoto phase oscillators supporting a chimera. We use the Ott/Antonsen ansatz to derive a nonlocal differential equation describing the network's dynamics in the limit of an infinite number of oscillators. We follow the chimera and bump states as the parameter is varied, describing many of the attractors of the network and the bifurcations they undergo. We find that there is not a simple deformation of a bump into a chimera; indeed, neither of these states persists over the whole range of the parameter. We find regions of multistability, and attractors including travelling waves, modulated travelling waves, spatially uniform periodic states and spatiotemporal chaos.

In Sec. II we present the different model networks considered and their continuum descriptions, and the hybrid model which interpolates between them. The results of numerical investigations are given in Sec. III. We conclude in Sec. IV.

II. MODELS STUDIED

We consider two systems, the first a network of theta neurons capable of supporting a stable bump solution, and the second a network of phase oscillators capable of supporting a stable chimera.

A. Theta neurons

The theta neuron is the normal form for a saddle-node-on-an-invariant-circle (SNIC) bifurcation[40–42]. Its state is given by a single angular variable, θ, and the neuron is said to fire when θ increases through π.

The network of N neurons is described by the equations

$$\frac{d\theta_j}{dt} = 1 - \cos\theta_j + (1+\cos\theta_j)(\eta_j + I_j) \tag{1}$$

for $j = 1, 2 \ldots N$ where the input to neuron j from other neurons in the network is

$$I_j = \frac{2\pi}{N} \sum_{k=1}^{N} G\left(\frac{2\pi|k-j|}{N}\right) P(\theta_k). \tag{2}$$

If uncoupled ($I_j = 0$) and $\eta_j < 0$, neuron j has two fixed points, one stable and one unstable. If uncoupled and $\eta_j > 0$ the neuron fires periodically with frequency $\sqrt{\eta_j}/\pi$. Thus there is a bifurcation from quiescence to periodic firing as the input to a neuron is increased.

We choose the coupling function $G(x) = 1 + A\cos x$ where A is a parameter, and

$$P(\theta) = \frac{8(1-\cos\theta)^5}{63} \tag{3}$$

as the pulsatile function with maximum at $\theta = \pi$, modelling the current pulse emitted as a neuron fires. The η_j are randomly chosen from a Lorentzian distribution with centre η_0 and half-width-at-half-maximum Δ. Similar networks have been considered in[42–44].

A typical bump state is shown in Fig. 1. There is a spatially-localised group of active neurons, centred approximately in the centre of the domain. Outside this bump the neurons are largely quiescent (i.e., their frequency is zero), as their input is not sufficient for them to fire. Note that the bump can be centred anywhere on the domain — its position is largely determined by the initial conditions. For this value of A ($A = 4$) the coupling function $G(x)$ is of Mexican-hat type: positive for small x and negative for larger x. For these parameters there also exists a stable "all-on" state for which most neurons are firing (except those with large and negative η_j); this state has no spatial structure (not shown).

B. Phase oscillators

The second system is a network of N phase oscillators described by

$$\frac{d\theta_j}{dt} = \eta_j - \frac{2\pi}{N} \sum_{k=1}^{N} G\left(\frac{2\pi|k-j|}{N}\right) \sin\left(\theta_j - \theta_k + \alpha\right) \tag{4}$$

for $j = 1, 2 \ldots N$, where the η_j and coupling function G are as above. The parameter α is a constant, and if uncoupled ($G = 0$) oscillator j would rotate at a constant speed η_j. Such systems have been considered in[16–20]. One significant difference between (4) and (1) is that the dynamics in (4) depend on *phase differences* only. Thus one can move to a rotating coordinate frame by replacing each θ_j by $\theta_j - \omega t$ and recover (4) but with η_0 increased by ω. Thus without loss of generality one can set $\eta_0 = 0$. Another manifestation of this invariance is that one can move to a rotating coordinate frame in which any synchronised oscillators are stationary.

An example of a chimera state for (4) is shown in Fig. 2. In panel (a) we see that the oscillators are in two groups: those near the boundary are synchronised (recall that the

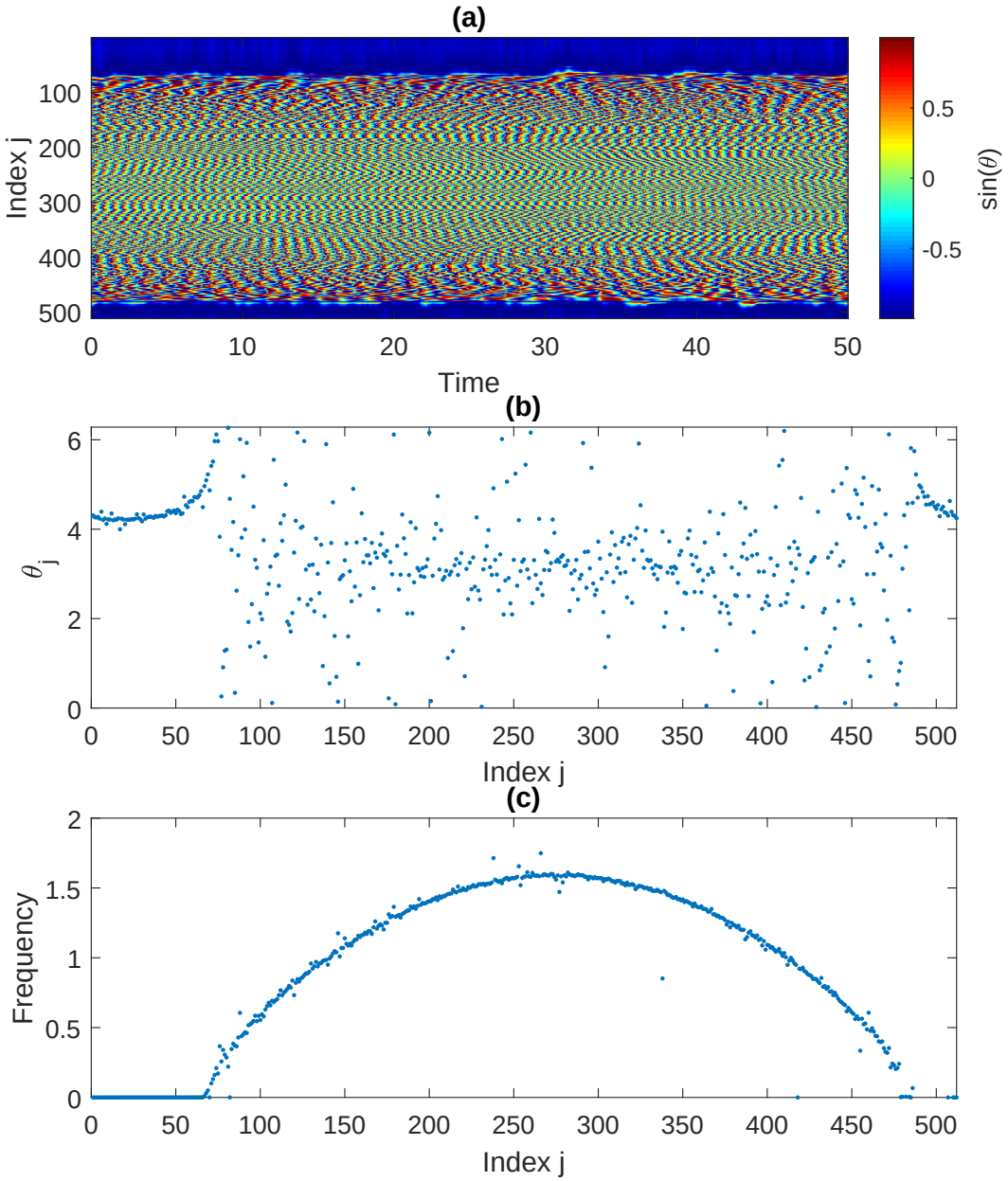

Figure 1. A bump state in (1)-(2). (a) $\sin\theta$ shown in colour. (b) snapshot of phases. (c) average frequency. Transients have been discarded and the average frequency for neuron j is calculated over 100 time units as $[\theta_j(100) - \theta_j(0)]/(200\pi)$. Parameters: $\eta_0 = -0.4, \Delta = 0.1, N = 512, A = 4$.

domain is periodic in space) while those in the centre of the domain are asynchronous. This is easier to see in panel (b) where we have gone to a coordinate frame rotating at the same speed as the synchronous oscillators, which now appear fixed. The difference is clear in the lower panels, where the average frequencies of oscillators in both the original (d) and corotating (e) frames are shown. Panel (c) shows a snapshot of phases but note that it is only *relative* phases which matter. The fact that the largely synchronous oscillators have

phase $\sim 4-5$ is just a result of when the snapshot was taken. This is in contrast to Fig. 1(b). It is the similarities between panels (a) and (c) in Fig. 1, and panels (b) and (e) in Fig. 2, respectively, which result in the conflation of chimeras and bumps, along with the similarities between (1) and (4).

For these parameters the "fully synchronised" state, in which the vast majority of oscillators have the same time-averaged frequency, is also stable (not shown).

C. Continuum description

Using standard theory[42–44] one can take the limit of (1) as $N \to \infty$ and describe the system by a probability density function $F(x, \eta, \theta, t)$ such that $F(x, \eta, \theta, t)d\eta\ d\theta$ is the probability that a neuron at position x has a value of η in $(\eta, \eta + d\eta)$ and phase in $(\theta, \theta + d\theta)$ at time t. Using the Ott/Antonsen ansatz[45,46] one can derive the evolution equation

$$\frac{\partial z(x,t)}{\partial t} = \frac{(i\eta_0 - \Delta)[1 + z(x,t)]^2 - i[1 - z(x,t)]^2}{2} + \frac{i[1 + z(x,t)]^2 I(x,t)}{2} \tag{5}$$

where

$$I(x,t) = \int_0^{2\pi} G(x-y)H(z(y,t))\ dy \tag{6}$$

and

$$H(z) = \frac{8}{63}\left[\frac{63}{8} - \frac{105}{16}(z+\bar{z}) + \frac{15}{4}(z^2+\bar{z}^2) - \frac{45}{32}(z^3+\bar{z}^3) + \frac{5}{16}(z^4+\bar{z}^4) - \frac{1}{32}(z^5+\bar{z}^5)\right] \tag{7}$$

$z(x,t)$ is the complex-valued order parameter at time t and position x:

$$z(x,t) = \int_{-\infty}^{\infty}\int_0^{2\pi} F(x,\eta,\theta,t)e^{i\theta}d\theta\ d\eta. \tag{8}$$

and overbar indicates the complex conjugate.

Similarly, one can take the limit $N \to \infty$ of (4) and obtain[19,47]

$$\frac{\partial z(x,t)}{\partial t} = -\Delta z(x,t) + \frac{1}{2}\left[R(x,t)e^{-i\alpha} - \bar{R}(x,t)e^{i\alpha}z^2(x,t)\right] \tag{9}$$

where

$$R(x,t) = \int_0^{2\pi} G(x-y)z(y,t)\ dy \tag{10}$$

and we have set $\eta_0 = 0$. Numerically solving (5)-(6) and (9)-(10) we obtain stable solutions consistent with those in Figs. 1 and 2, respectively (not shown).

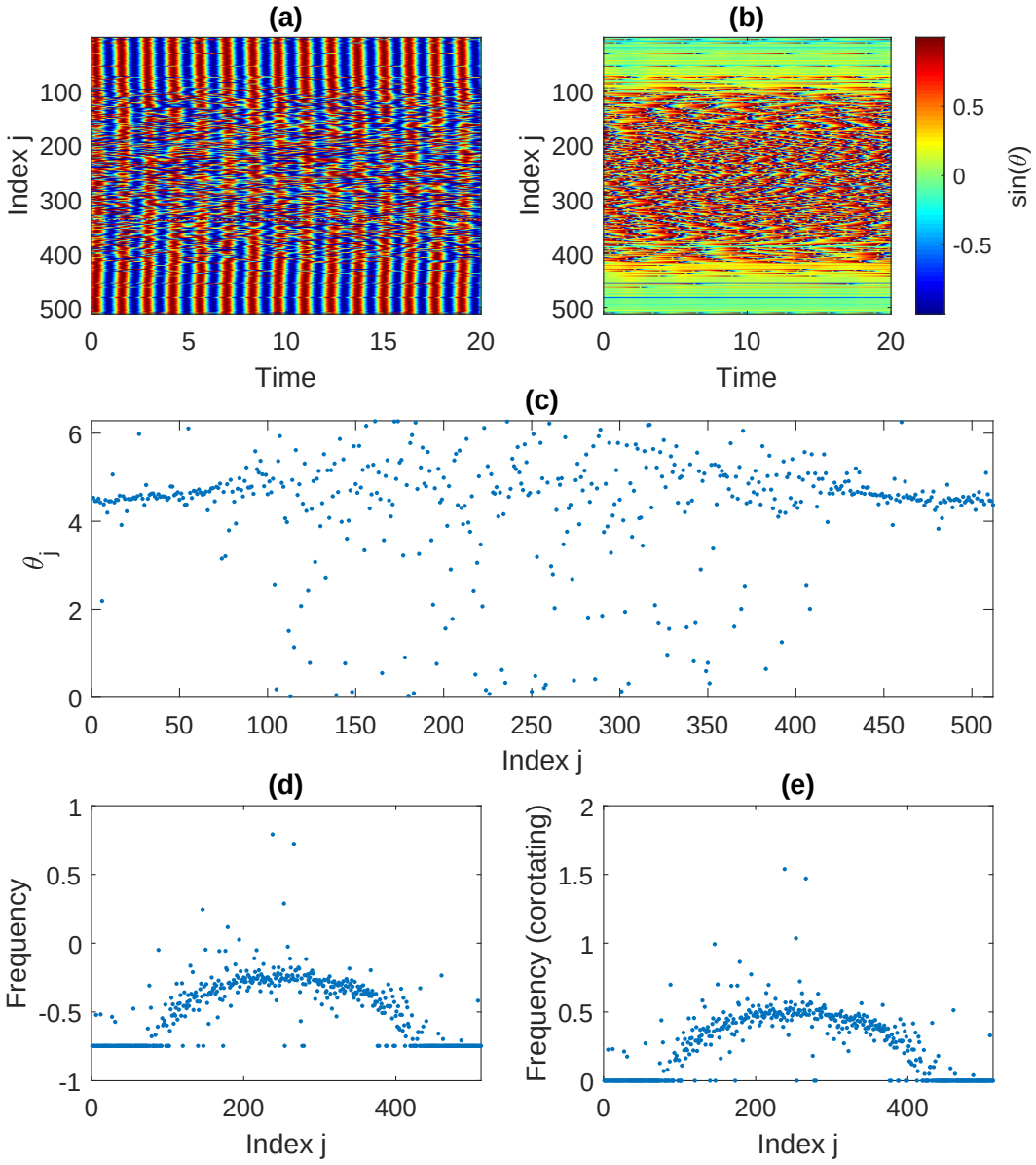

Figure 2. A chimera state in (4). (a) $\sin\theta$ shown in colour. (b) $\sin\theta$ shown in colour in a rotating coordinate frame. The same colourbar applies to panels (a) and (b). (c) snapshot of phases. (d) average frequency of oscillators. (e) average frequency of oscillators in a rotating coordinate frame. Transients have been discarded and the average frequency for an oscillator is calculated as in Fig. 1. Parameters: $\eta_0 = 0, \Delta = 0.1, N = 512, A = 0.9, \alpha = \pi/2 - 0.2$.

D. Hybrid model

We now consider a system which linearly interpolates between (5) and (9). This is chosen to be

$$\begin{aligned}\frac{\partial z}{\partial t} =&(1-p)\left\{\frac{(i\eta_0-\Delta)[1+z(x,t)]^2-i[1-z(x,t)]^2}{2}+\frac{i[1+z(x,t)]^2 I(x,t)}{2}\right\}\\ &+p\left\{-\Delta z(x,t)+\frac{1}{2}\left[R(x,t)e^{-i\alpha}-\bar{R}(x,t)e^{i\alpha}z^2(x,t)\right]\right\}\end{aligned} \tag{11}$$

with $G(x)=1+(4-3.1p)\cos x$, and R and I as above. When $p=0$ this reduces to (5)-(6) and when $p=1$, to (9)-(10). Of course, this is not the only way in which to interpolate between (5) and (9) but we choose it to be perhaps the simplest. The corresponding hybrid model of discrete oscillators is

$$\begin{aligned}\frac{d\theta_j}{dt} =&(1-p)\left[1-\cos\theta_j+(1+\cos\theta_j)(\eta_j+I_j)\right]\\ &+p\left[\eta_j-\frac{2\pi}{N}\sum_{k=1}^{N}G\left(\frac{2\pi|k-j|}{N}\right)\sin\left(\theta_j-\theta_k+\alpha\right)\right]\end{aligned} \tag{12}$$

with G as above and I_j as in (2). Note that this model does not have any specific biological interpretation; it is created to interpolate between two well-known systems.

To understand the transition from the bump supported by (5)-(6) and the chimera supported by (9)-(10) we first solve (11) while quasistatically increasing p from 0 to 1 over 5000 time units, starting at the stable bump. The result is shown in Fig. 3(a). We see that the bump persists to $p\approx 0.25$, at which point the system jumps to a spatially-uniform state. A pattern emerges at $p\approx 0.45$ and several types of solution are seen before a chimera appears just before $p=1$.

Quasistatically decreasing p from 1 to 0 over 5000 time units (starting at a chimera) we obtain Fig. 3(b). The chimera persists to $p\approx 0.85$ at which point other spatiotemporal patterns arise. A spatially-uniform state appears for $0.25<p<0.35$ and a stable bump state finally appears at $p\approx 0.12$. There seem to be regions of multistability, and it is clear that the bump does not smoothly deform into a chimera or vice versa. This paper is devoted to understanding the sequence of bifurcations that occur as p is varied in order to explain the results in Fig. 3.

III. RESULTS

We will analyse various types of solution and piece together the results at the end of this section. Numerical solutions of (11) were obtained by discretising space in either 256 or 512 equally spaced points and using the FFT to implement the convolutions in (6) and (10). Pseudoarclength continuation[48,49] was used to follow solutions as p was varied, and stability was determined from the eigenvalues of the linearisation about a state.

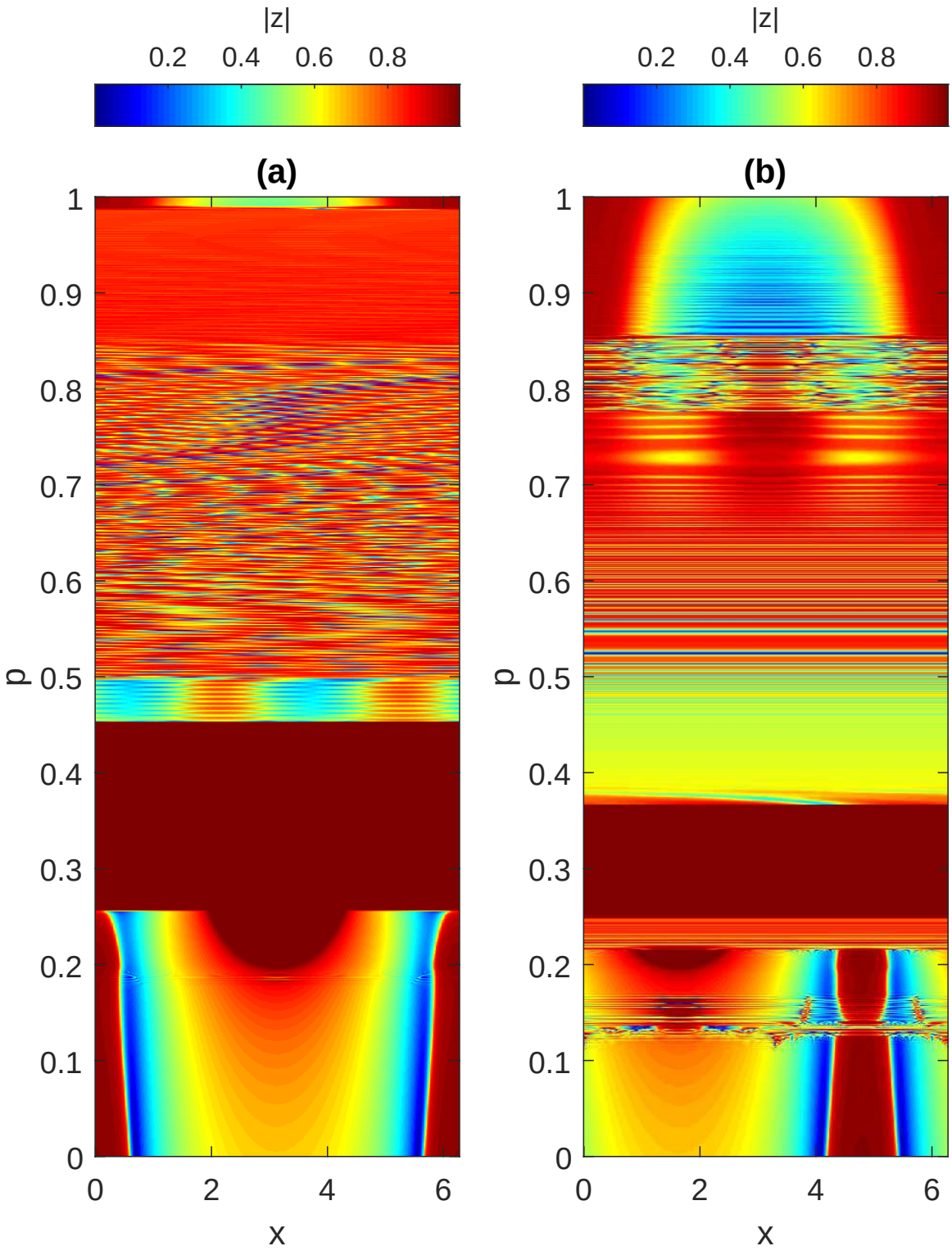

Figure 3. Solutions of (11) as p is increased from 0 to 1 in time (a) and decreased from 1 to 0 in time (b). When $p = 0$ the systerm supports a bump, whereas for $p = 1$ it supports a chimera. Other parameters: $\eta_0 = -0.4, \Delta = 0.1, \alpha = \pi/2 - 0.2$. 512 spatial points were used.

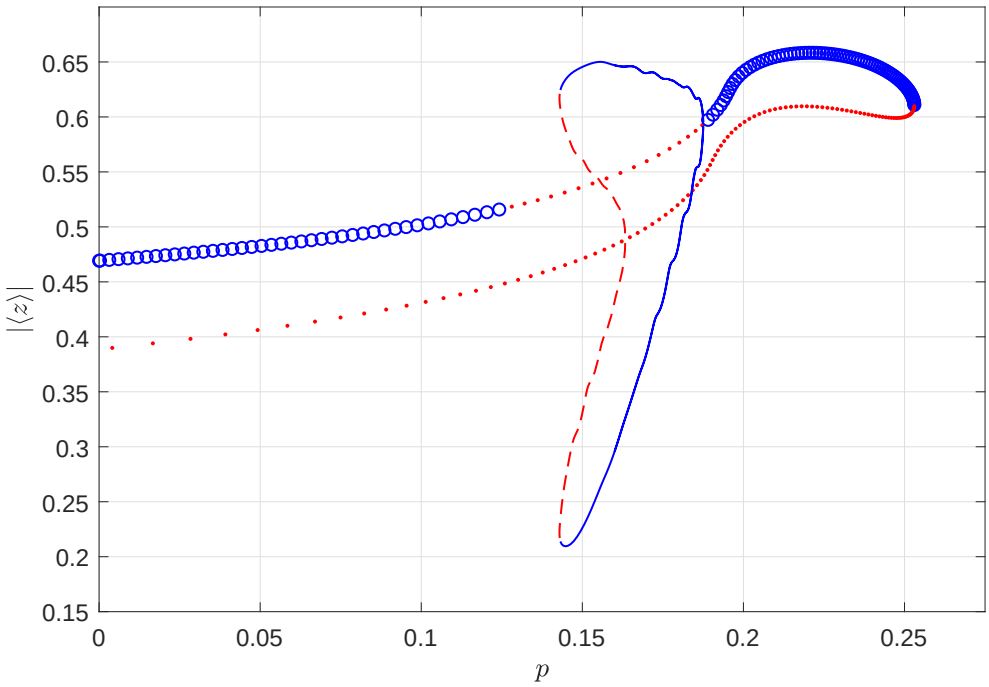

Figure 4. Stationary and periodic bump solutions of (11). $\langle z\rangle$ is the mean over x of $z(x,t)$. For stationary bump solutions (circles and dots) we plot $|\langle z\rangle|$ while for periodic bump solutions (dashed and solid curves) we plot the maximum and minimum over one period of $|\langle z\rangle|$. Blue: stable, red: unstable. Parameters as in Fig. 3.

A. Bump

Continuing the stable bump state that exists at $p = 0$ we obtain Fig. 4. It undergoes two Hopf bifurcations, the second one supercritical, as p is increased before being destroyed in a saddle-node bifurcation at $p \approx 0.253$. The rightmost Hopf bifurcation creates a stable periodic orbit at $p \approx 0.187$, and an unstable periodic orbit is created in a Hopf bifurcation from the unstable branch of bumps at $p \approx 0.163$. These two are destroyed in a saddle-node bifurcation of periodic orbits at $p \approx 0.143$.

There is a gap in Fig. 4 for $0.125 < p < 0.143$ where the attractor is not shown. Simulations suggest that the leftmost Hopf bifurcation is subcritical, and there are spatiotemporally chaotic solutions over this range of values of p, with an example shown in Fig. 5. Windows of periodic or chaotic solutions are visible for $0.1 < p < 0.2$ in both panels of Fig. 3, and the saddle-node bifurcation destroying the stationary bump at $p \approx 0.253$ is seen in the left panel.

Note that another "bump" state disconnected from the branches shown here is found for $p \sim 0.4$; see Sec. III D.

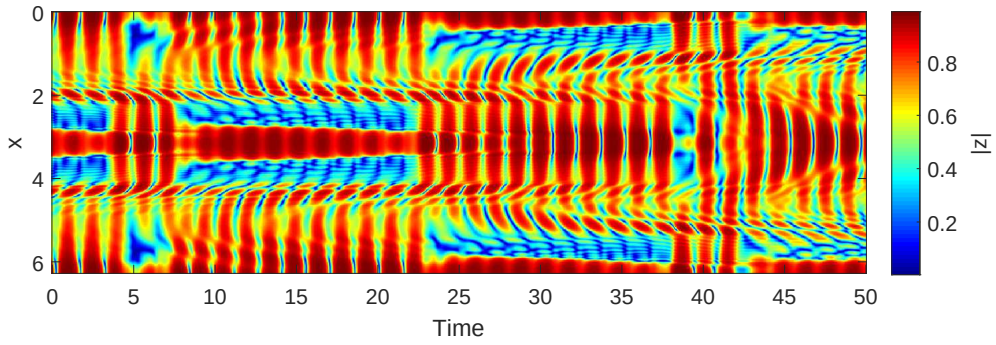

Figure 5. A chaotic solution of (11) at $p = 0.14$. $|z(x,t)|$ is shown in colour. Parameters as in Fig. 3.

B. Chimera/standing wave

For $p = 1$ the chimera is a fixed point in a uniformly rotating coordinate frame, but for smaller p it is a periodic orbit in the original coordinate frame and must be studied as such. Following the chimera from $p = 1$ we obtain the results in Fig. 6, shown as blue circles. This state undergoes a Neimark-Sacker bifurcation as p is decreased, leading to quasiperiodic solutions, discussed below. The branch of chimera solutions undergoes four saddle-node bifurcations, becoming stable on the fourth one. On the stable branch the magnitude of spatial variation in structure decreases until the state is destroyed in a collision with the spatially-uniform periodic state. Solutions on the stable branch around $p = 0.7$ appear as standing waves; see Fig. 7 for an example. The spatially-uniform periodic state is stable at $p = 1$ and goes unstable in a subcritical bifurcation as p is decreased. It then stabilises in a supercritical bifurcation in which the stable standing wave solution is created. There is another subcritical bifurcation as p is decreased before the unstable spatially-uniform periodic state is destroyed when it collides with a spatially-uniform steady state in a Hopf bifurcation from this state (see Fig. 9).

The stable spatially-uniform periodic state at $p = 1$ is a spatially uniform steady state in a uniformly rotating coordinate frame. It corresponds to the "fully synchronised" state, which is one of the two attractors of (9). At $p \approx 0.78$ the stable standing wave is destroyed in a saddle-node bifurcation and this leads to the creation of a chaotic attractor via intermittency[50], as shown in Fig. 8. The chaotic behaviour persists up to $p \approx 0.92$; see Sec. III E.

C. Spatially-uniform steady states

Following the spatially-uniform steady state that is stable for $p = 0$ we obtain Fig. 9. Recall that at $p = 0$ it is the stable "all-on" solution of (5). This branch persists until $p = 1$

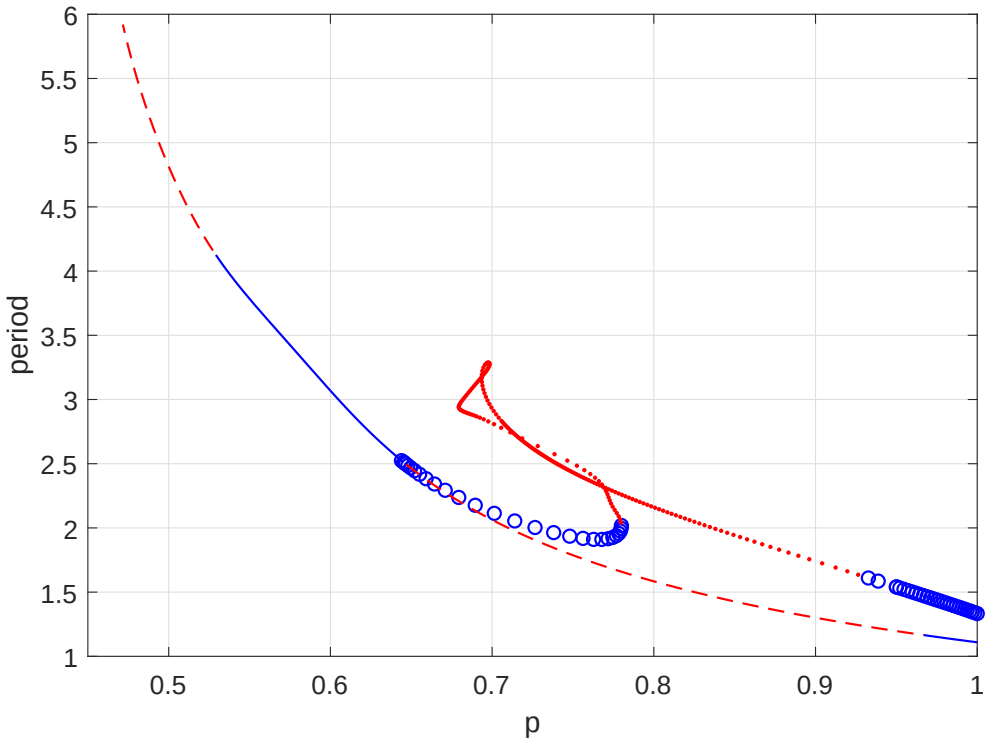

Figure 6. Period of the standing wave/chimera (circles and dots) and of the spatially-uniform periodic state (dashed and solid curve) solutions of (11). The left endpoint corresponds to the creation of the branch of spatially-uniform periodic states in a Hopf bifurcation from a spatially-uniform steady state (see Fig. 9). Blue: stable, red: unstable. Parameters as in Fig. 3.

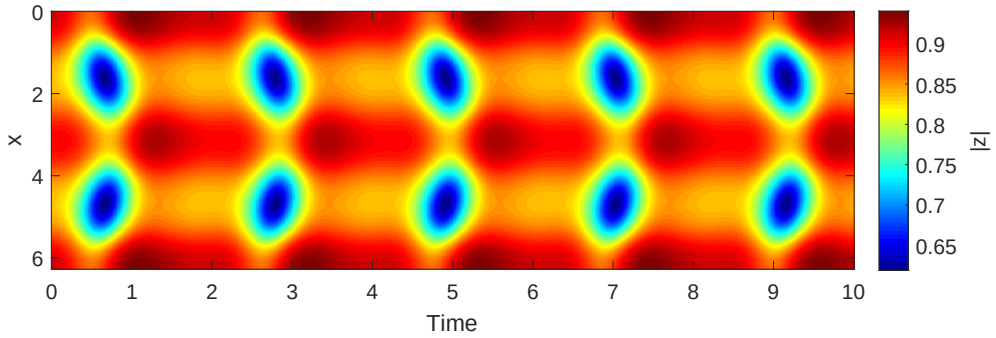

Figure 7. An example of a standing wave solution of (11) at $p = 0.7$. $|z(x,t)|$ is shown in colour. Parameters as in Fig. 3.

and when $p = 1$ it is the zero state, an unstable fixed point of (9). The solution which is stable for $p = 0.3$ goes unstable as p is increased just before the saddle-node bifurcation that can be seen in Fig. 9. This is a Turing bifurcation, i.e. the Jacobian of the system evaluated at the fixed point has a zero eigenvalue and a corresponding eigenvector with spatial structure. This

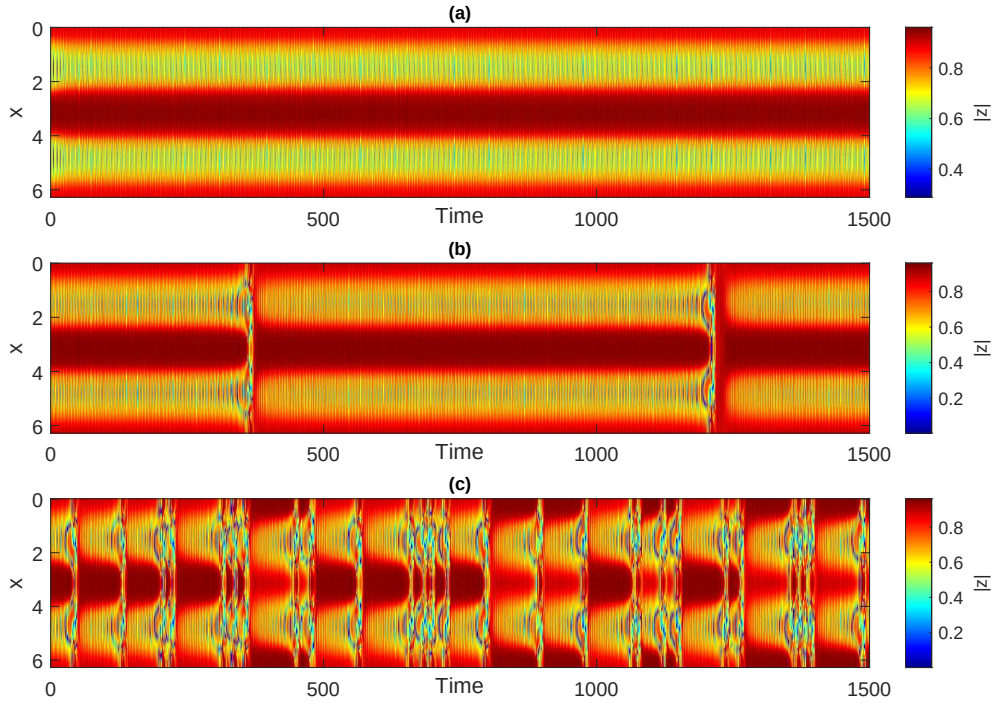

Figure 8. The onset of chaotic behaviour via intermittency. (a) Standing wave solution of (11) at $p = 0.775$; chaotic solutions at (b) $p = 0.78$ and (c) $p = 0.784$. $|z(x,t)|$ is shown in colour. Parameters as in Fig. 3.

bifurcation creates an unstable bump seen in Fig. 12. There is another Turing bifurcation at $p \approx 0.251$ which seems subcritical. There is a small window ($0.251 \leq p \leq 0.253$) in which the system has the two attractors: a spatially-uniform steady state and the stable bump shown in Fig. 4. For the solution in Fig. 9 there is a dynamic Turing instability at $p \approx 0.035$, i.e., the Jacobian has a complex conjugate pair of purely imaginary eigenvalues and corresponding eigenvectors with spatial structure. This bifurcation is supercritical, resulting in a travelling wave, which goes unstable to a modulated travelling wave at $p \approx 0.046$. This modulated travelling wave becomes chaotic at $p \approx 0.061$ and this chaos persists until $p \approx 0.101$.

D. Travelling waves

For some values of p, e.g. $p = 0.48$, we obtain travelling waves, as shown in the top two panels of Fig. 10. They have a constant profile which travels at a constant speed and are thus fixed points of

$$\begin{aligned}\frac{\partial z}{\partial t} =&(1-p)\left\{\frac{(i\eta_0-\Delta)[1+z(x,t)]^2-i[1-z(x,t)]^2}{2}+\frac{i[1+z(x,t)]^2 I(x,t)}{2}\right\}\\ &+p\left\{-\Delta z(x,t)+\frac{1}{2}\left[R(x,t)e^{-i\alpha}-\bar{R}(x,t)e^{i\alpha}z^2(x,t)\right]\right\}+c\frac{\partial z}{\partial x}\end{aligned} \tag{13}$$

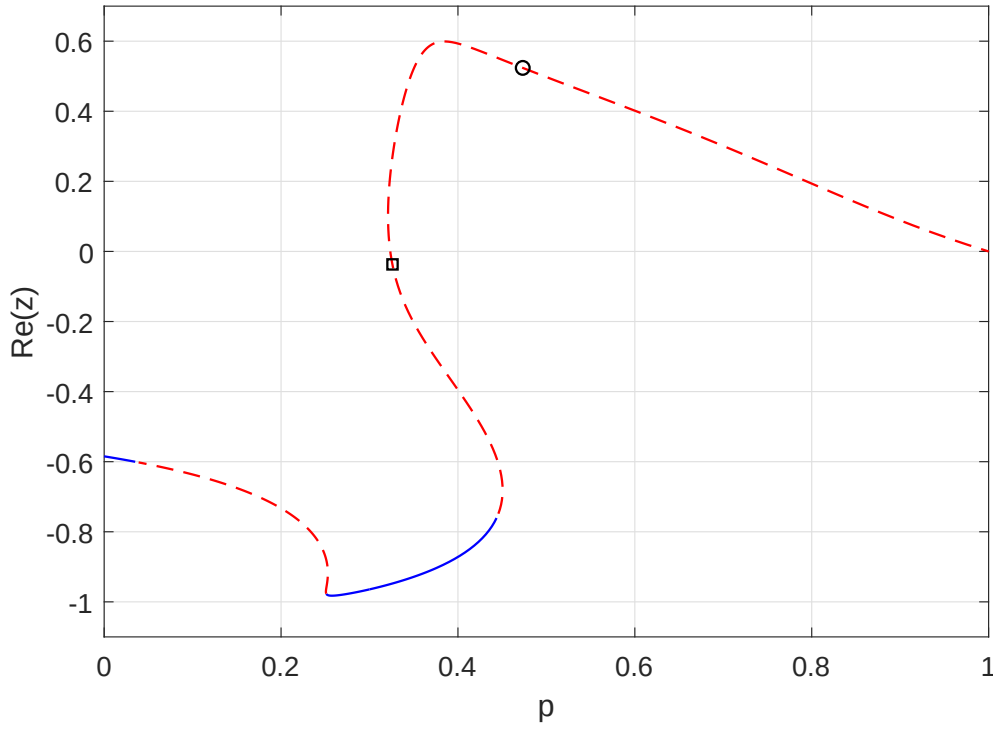

Figure 9. Spatially uniform steady states of (11) (Re(z) is plotted). Solid: stable; dashed: unstable. The circle marks the Hopf bifurcation creating the spatially-uniform periodic state shown in Fig. 6. The square marks the Turing bifurcation creating the bump state seen in Fig. 12. Parameters as in Fig. 3.

where c is their speed[44,51]. (Any spatial shift of such a fixed point is also a fixed point of (13), so we have to append a scalar equation to (13) which has the effect of selecting one from this continuum.) Having found a fixed point of (13) one can determine its stability by linearising (13) about it.

Following these travelling waves we obtain Fig. 11. The branch of solutions is created by branching off a stationary bump with speed 0 at $p \approx 0.437$. The branch of stationary bumps is shown in Fig. 12. (We refer to these stationary solution as "bumps" as they are stationary and $|z|$ is a unimodal function of x for them, but there is little variation in $|z|$ over x.) Referring to Fig. 11 there are bifurcations of travelling waves at p values of $0.905, 0.83, 0.502, 0.455, 0.44$ and 0.373. The first five are Hopf bifurcations and the last one is a saddle-node bifurcation. The leftmost four Hopf bifurcations create modulated travelling waves, an example of which is shown in the lower two panels of Fig. 10.

To investigate the modulated travelling waves we define

$$W(t) = \mathrm{Re}\{z(0,t)\} - \frac{1}{2\pi}\int_0^{2\pi} \mathrm{Re}\{z(x,t)\}dx. \tag{14}$$

For a fixed value of p we integrate (11) for 1300 time units, then for another 1000 time

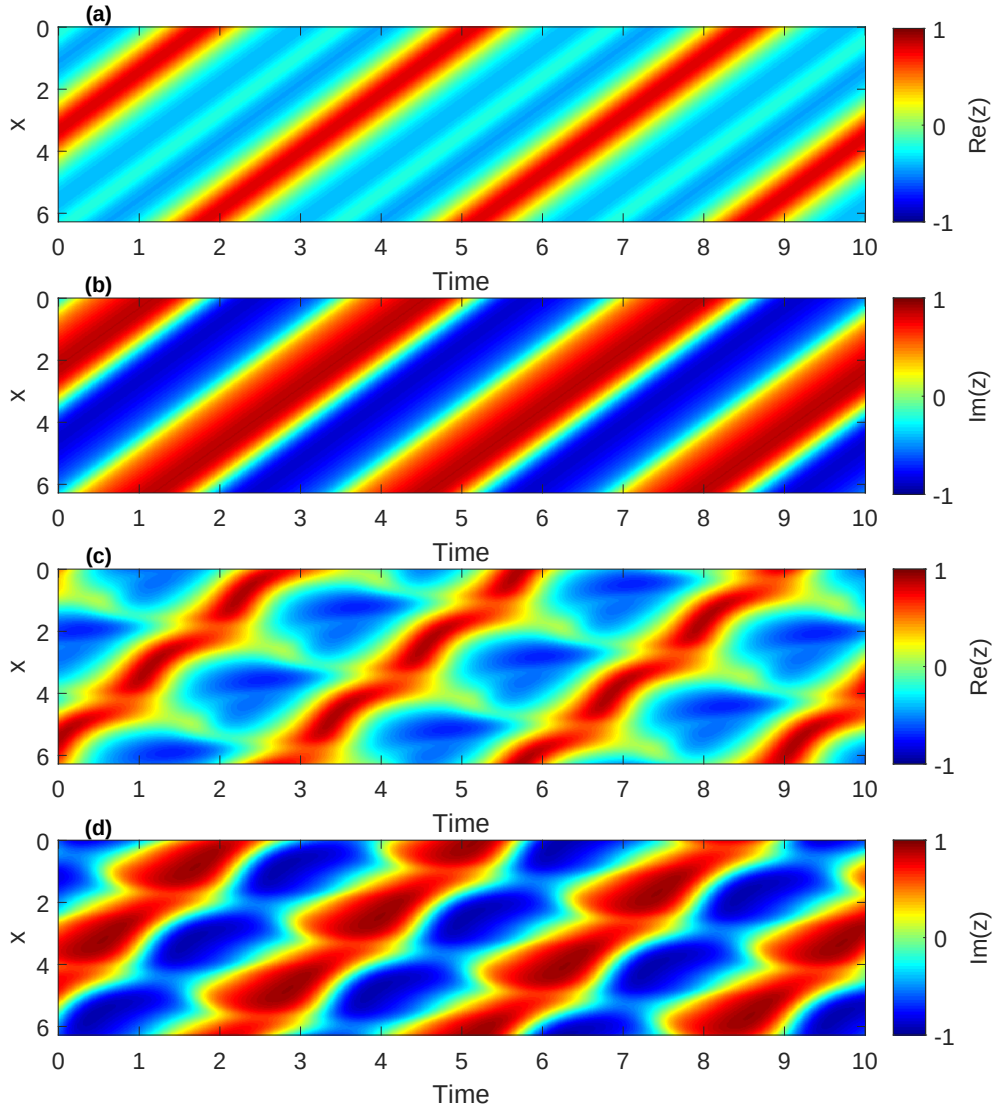

Figure 10. A travelling wave solution of (11) is shown in (a) and (b): real and imaginary parts of z, respectively, for $p = 0.48$. A modulated travelling wave solution is shown in (c) and (d): the real and imaginary parts of z, respectively, for $p = 0.6$. Parameters as in Fig. 3.

units, recording $\mathrm{Re}\{z(0,t)\}$ every time W increases through zero. These values are plotted in Fig. 13, where in panel (a) we have quasistatically increased p while in panel (b) we have decreased it. For a smoothly travelling wave all of these values at a fixed p will be the same, while for a modulated wave they will have a range of values. The results are consistent with those in Fig. 11, but there are some regions of bistability with both a travelling wave and a modulated travelling wave being stable, for example, $0.83 < p < 0.84$ and $0.455 < p < 0.493$.

The rightmost Hopf bifurcation at $p \approx 0.905$ appears to be subcritical and as p is increased through this value while following the travelling wave, the system jumps to the coexisting chaotic attractor (see below).

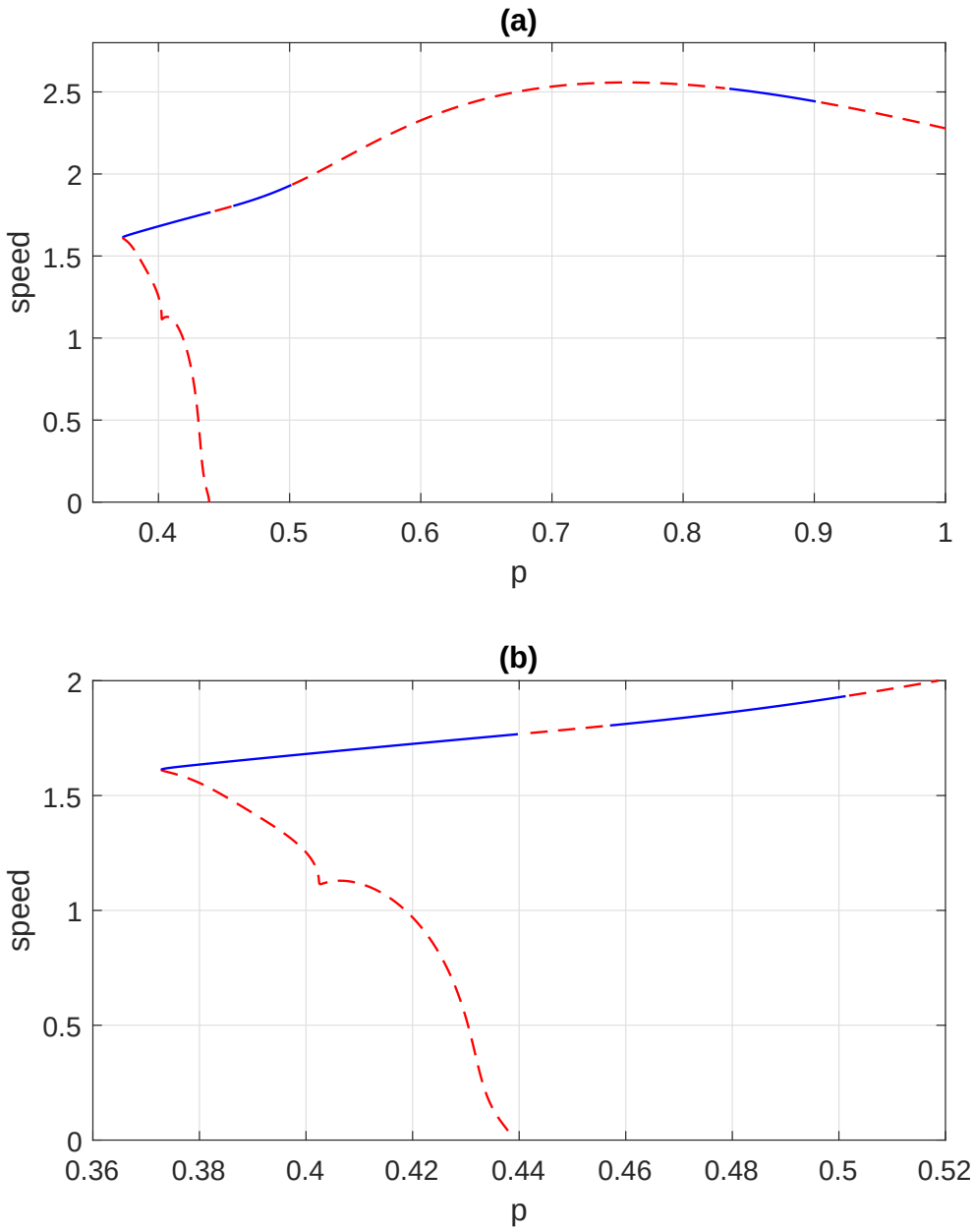

Figure 11. The speed of a travelling wave solution of (11). These solutions are fixed points of (13), where c is the speed. Solid: stable; dashed: unstable. Panel (b) is a zoom of panel (a). The solution branches off a stationary bump (see Fig. 12) at zero speed. Parameters as in Fig. 3.

E. Chaos

As mentioned above, the stable standing wave is destroyed in a saddle-node bifurcation at $p \approx 0.78$, leading to chaotic behaviour via intermittency. Following that attractor as p is increased further and visualising the solutions using a Poincaré map as in the previous section, we obtain Fig. 14 (a). Coming from the right we see that the stable chimera

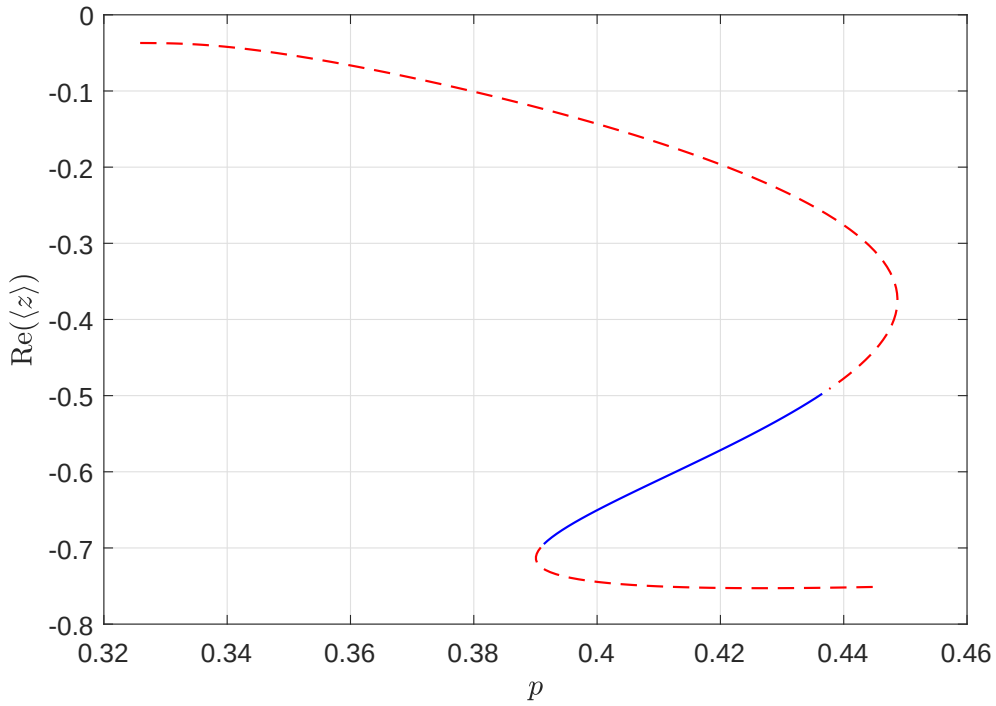

Figure 12. Stationary bump states of (11). The real part of $\langle z \rangle$ (the mean over x of $z(x,t)$) is plotted. Solid: stable, dashed: unstable. The rightmost bifurcation (indicated by the change in stability) creates the travelling wave in Fig. 11. The leftmost bifurcation seems to be a subcritical Hopf bifurcation. Both endpoints of this branch correspond to creation of this branch in a Turing bifurcation from the spatially uniform state shown in Fig. 9. Parameters as in Fig. 3.

undergoes a Hopf bifurcation at $p \approx 0.93$ leading to quasiperiodic behaviour, which then becomes chaotic at $p \approx 0.92$. This persists down to $p \approx 0.78$, although with a number of windows in which the behaviour is quasiperiodic. Panel (b) of Fig. 14 shows the largest Lyapunov exponent of the solution shown in panel (a), confirming its chaotic nature.

F. Summary

We summarise the dynamics in Table I and Fig. 15. Note that this is not an exact description as, for example, the bands of quasiperiodic behaviour seen in Fig. 14 are not described, but lumped together as "chaos".

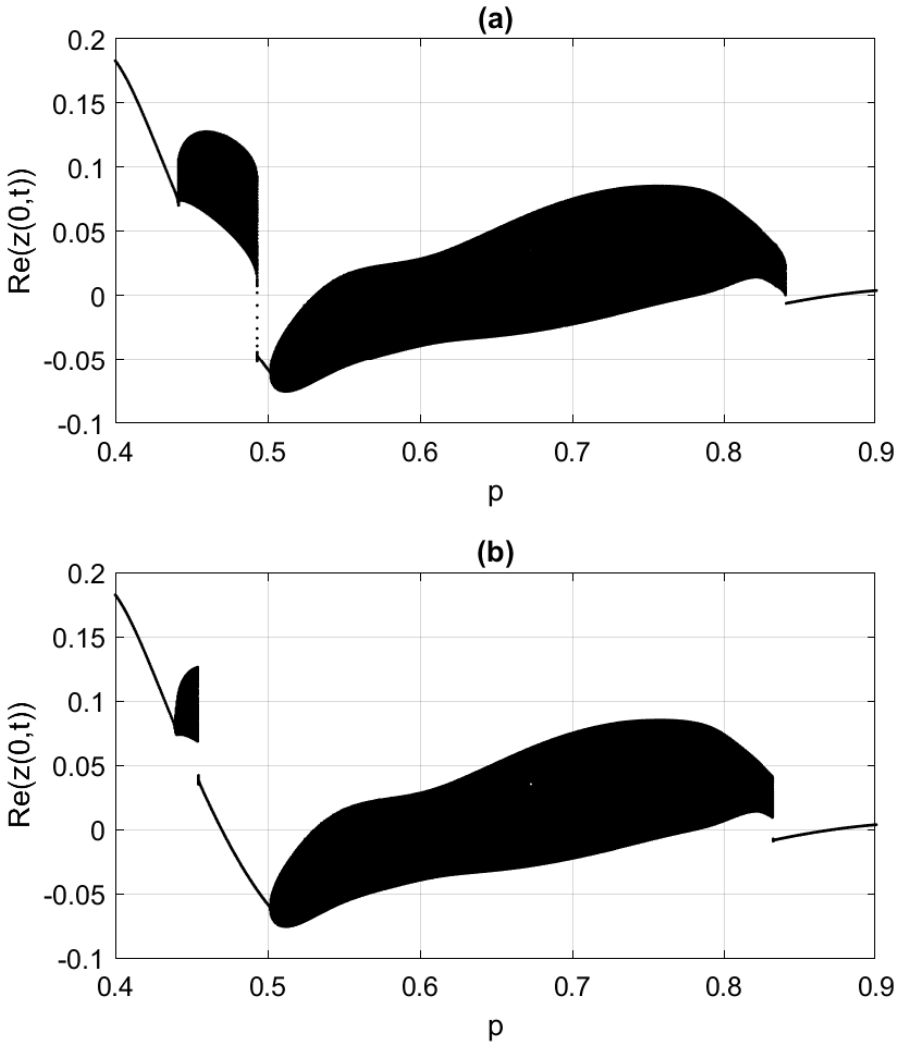

Figure 13. Poincaré maps representing solutions of (11) for (a) increasing p and (b) decreasing p. Travelling waves (one point for a particular value of p) and modulated travelling waves (many points for a particular value of p) are shown. Parameters as in Fig. 3.

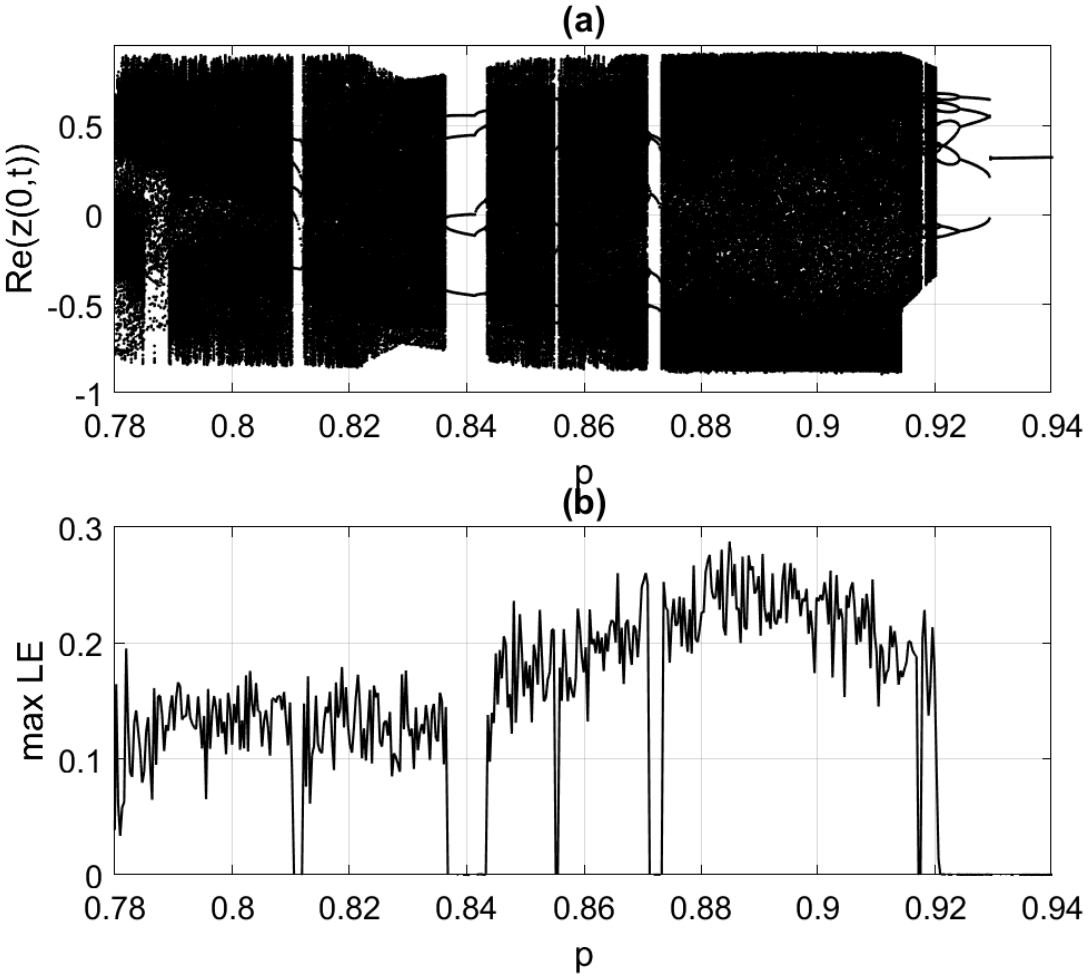

Figure 14. (a) Poincaré map representing chaotic solutions of (11). (b) Maximum Lyapunov exponent for the solution in (a). Parameters as in Fig. 3.

Table I. Summary of dynamics.

Range of p	Stable Solutions
0 – 0.035	bump and spatially-uniform steady state ("all-on")
0.035 – 0.046	bump and travelling wave
0.046 – 0.061	bump and modulated travelling wave
0.061 – 0.101	bump and chaos
0.101 – 0.125	bump
0.125 – 0.143	chaos
0.143 – 0.187	breathing bump
0.187 – 0.251	bump
0.251 – 0.253	spatially-uniform steady state and bump
0.253 – 0.373	spatially-uniform steady state
0.373 – 0.391	spatially-uniform steady state and travelling wave
0.391 – 0.437	spatially-uniform steady state and travelling wave and stationary bump
0.437 – 0.44	spatially-uniform steady state and travelling wave
0.44 – 0.445	spatially-uniform steady state and modulated travelling wave
0.445 – 0.455	modulated travelling wave
0.455 – 0.493	travelling wave and modulated travelling wave
0.493 – 0.502	travelling wave
0.502 – 0.528	modulated travelling wave
0.528 – 0.645	spatially-uniform periodic and modulated travelling wave
0.645 – 0.78	standing wave and modulated travelling wave
0.78 – 0.83	modulated travelling wave and chaos
0.83 – 0.84	travelling wave and modulated travelling wave and chaos
0.84 – 0.905	travelling wave and chaos
0.905 – 0.92	chaos
0.92 – 0.93	quasiperiodic chimera
0.93 –0.965	chimera
0.965 – 1	spatially-uniform periodic and chimera

Simulations of the hybrid discrete system (12) at fixed values of p show behaviour consistent with all of the results presented in Secs. III A-III D (not shown). We show simulations of the hybrid discrete system (12) as p is swept from 0 to 1 over 5000 time units, starting with a bump, in panel (a) of Fig. 16. Panel (b) shows the result of decreasing p from 1 to 0 over the same amount of time, starting with a chimera. In order to compare with Fig. 3 we

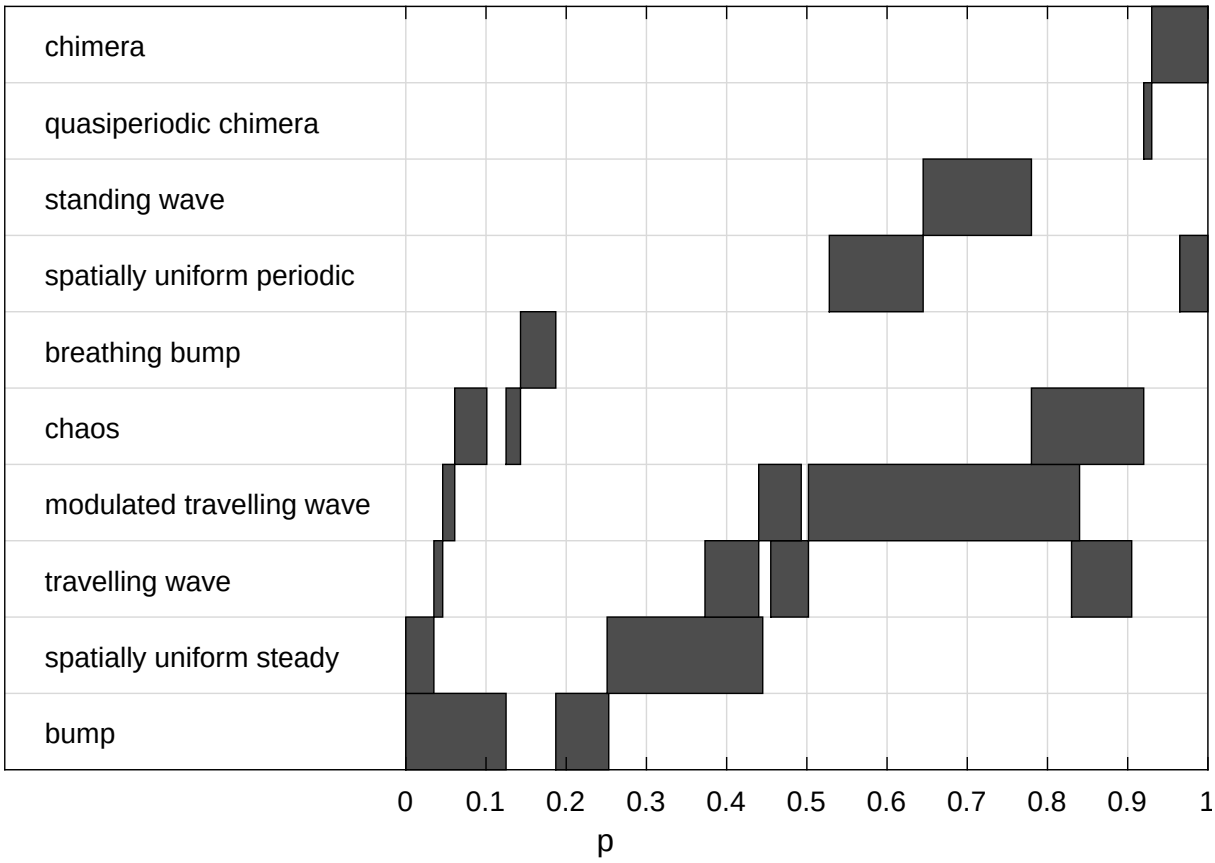

Figure 15. A graphical representation of the results in Table I. The filled bars show the ranges of p for which the corresponding type of solution is stable. Note the stable bump and spatially uniform steady state at $p = 0$, and the stable chimera and spatially uniform periodic state (which is stationary in a rotating coordinate frame) at $p = 1$.

define an order parameter

$$Y_j(t) = \frac{1}{201} \sum_{k=j-100}^{j+100} e^{i\theta_k} \tag{15}$$

and plot its absolute value in Fig. 16.

Comparing the left panels Figs. 3 and 16, starting from $p = 0$ we see very good agreement until $p \approx 0.14$. In Fig. 16 the bump "jumps" to a different part of the domain at this value of p, and the central red strip in Fig. 16 for $0.14 < p < 0.25$ corresponds to that on the boundaries of the domain in Fig. 3. Increasing p, the agreement is very good except that the system in Fig. 3 does not move to a chimera until p is close to 1, unlike in Fig. 16.

Comparing the right panels as p is decreased, the agreement is good until $p \approx 0.9$, where the chimera in the discrete network is lost, but persists in the continuum system. For smaller values of p most features of the figures match qualitatively, with transitions occurring at similar values of p.

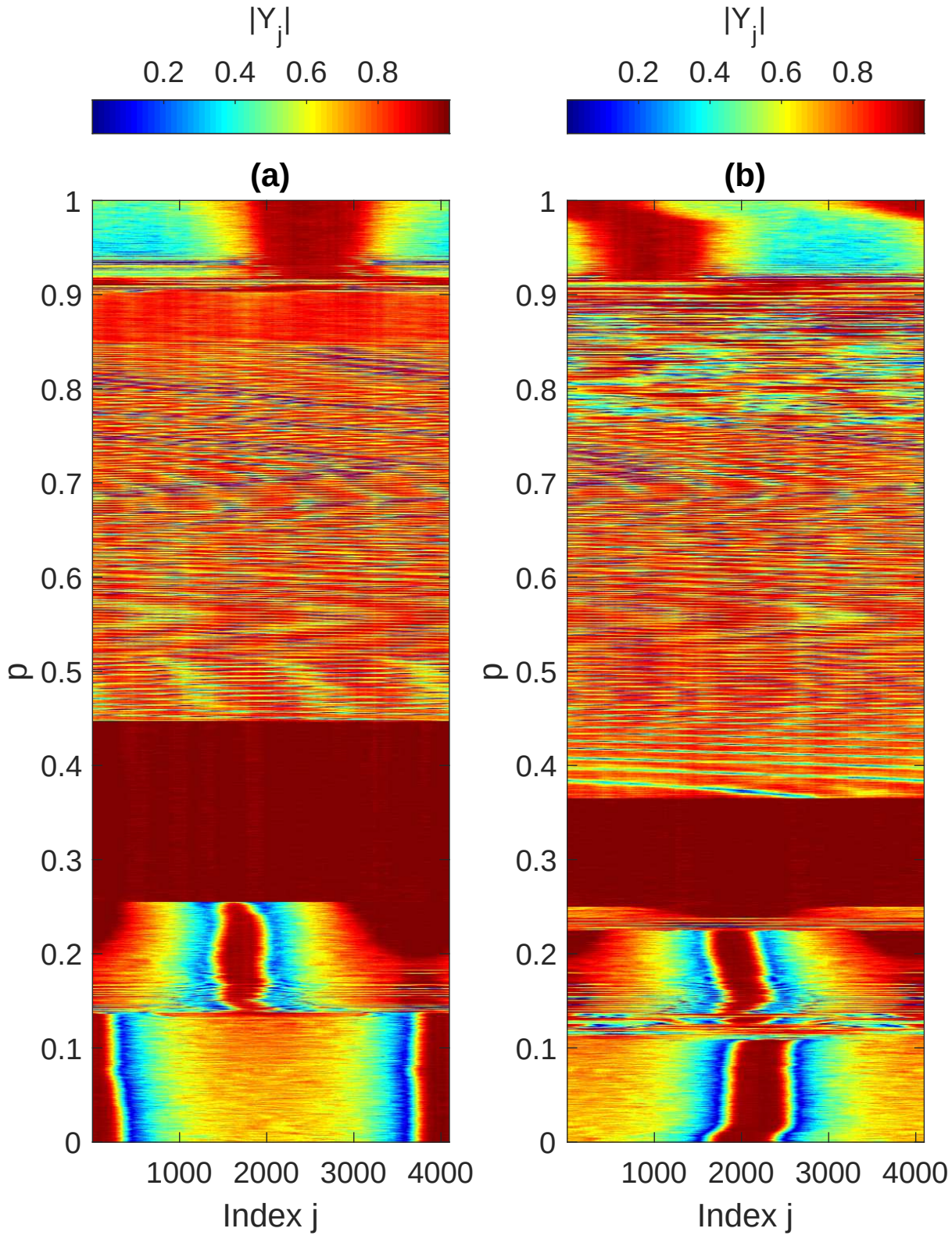

Figure 16. Solutions of (12) as p is increased from 0 to 1 in time (a) and decreased from 1 to 0 in time (b). Y_j is defined in the text. $N = 4096$ and other parameters as in Fig. 3.

IV. DISCUSSION

We have thoroughly investigated the dynamics of (11), an equation which linearly interpolates between the continuum description of a network of theta neurons supporting a bump and a network of phase oscillators supporting a chimera. The bump which exists and is stable for $p = 0$ only persists up to $p \approx 0.253$ and is not stable over all of this range. The stable chimera which exists at $p = 1$ persists down to $p \approx 0.645$ but is not stable over this whole range either, and is significantly deformed into a standing wave as p is decreased. Thus there is not a smooth deformation from a chimera to a bump state. In fact, the only solution which persists over the whole range $p \in [0, 1]$ is the stationary spatially uniform state, which is the (unstable) zero state at $p = 1$ and the "all on" state at $p = 0$.

We have found a rich variety of other solutions including spatiotemporal chaos, travelling waves, and modulated travelling waves. Of course there are many ways to interpolate between (5) and (9) and it may be possible to find another interpolation such that a bump does deform smoothly into a chimera, or one in which the equivalent of Table I is simpler, but we leave that for future work.

Data availability: Data sharing is not applicable to this article as no new data were created or analyzed in this study.

Conflicts of Interest: The authors have no conflicts to disclose.

REFERENCES

[1]D. B. Poll, K. Nguyen, and Z. P. Kilpatrick, "Sensory feedback in a bump attractor model of path integration," Journal of computational neuroscience **40**, 137–155 (2016).

[2]C. R. Laing, W. C. Troy, B. Gutkin, and G. B. Ermentrout, "Multiple bumps in a neuronal model of working memory," SIAM Journal on Applied Mathematics **63**, 62–97 (2002).

[3]K. Wimmer, D. Q. Nykamp, C. Constantinidis, and A. Compte, "Bump attractor dynamics in prefrontal cortex explains behavioral precision in spatial working memory," Nature neuroscience **17**, 431–439 (2014).

[4]S.-i. Amari, "Dynamics of pattern formation in lateral-inhibition type neural fields," Biological cybernetics **27**, 77–87 (1977).

[5]P. C. Bressloff, "Spatiotemporal dynamics of continuum neural fields," Journal of Physics A: Mathematical and Theoretical **45**, 033001 (2012).

[6]S. Coombes, "Waves, bumps, and patterns in neural field theories," Biol. Cybern. **93**, 91–108 (2005).

[7]S. Coombes, H. Schmidt, and I. Bojak, "Interface dynamics in planar neural field models," The Journal of Mathematical Neuroscience (JMN) **2**, 1–27 (2012).

[8]P. C. Bressloff and Z. P. Kilpatrick, "Two-dimensional bumps in piecewise smooth neural fields with synaptic depression," SIAM Journal on Applied Mathematics **71**, 379–408 (2011).

[9]D. J. Pinto and G. B. Ermentrout, "Spatially structured activity in synaptically coupled neuronal networks: II. Lateral inhibition and standing pulses," SIAM Journal on Applied Mathematics **62**, 226–243 (2001).

[10]B. Ermentrout, "Neural networks as spatio-temporal pattern-forming systems," Rep. Prog. Phys. **61**, 353–430 (1998).

[11]P. Blomquist, J. Wyller, and G. T. Einevoll, "Localized activity patterns in two-population neuronal networks," Physica D: Nonlinear Phenomena **206**, 180–212 (2005).

[12]X.-J. Wang, "Synaptic reverberation underlying mnemonic persistent activity," Trends in Neurosciences **24**, 455 – 463 (2001).

[13]C. Laing and C. Chow, "Stationary bumps in networks of spiking neurons," Neural Comput. **13**, 1473–1494 (2001).

[14]A. Compte, N. Brunel, P. S. Goldman-Rakic, and X.-J. Wang, "Synaptic mechanisms and network dynamics underlying spatial working memory in a cortical network model," Cerebral Cortex **10**, 910–923 (2000).

[15]B. S. Gutkin, C. R. Laing, C. L. Colby, C. C. Chow, and G. B. Ermentrout, "Turning on and off with excitation: the role of spike-timing asynchrony and synchrony in sustained neural activity," Journal of computational neuroscience **11**, 121–134 (2001).

[16]D. Abrams and S. Strogatz, "Chimera states for coupled oscillators," Phys. Rev. Lett. **93**, 174102 (2004).

[17]D. Abrams and S. Strogatz, "Chimera states in a ring of nonlocally coupled oscillators," Int. J. Bifurcat. Chaos **16**, 21–37 (2006).

[18]Y. Kuramoto and D. Battogtokh, "Coexistence of Coherence and Incoherence in Nonlocally Coupled Phase Oscillators," Nonlinear Phenom. Complex Syst **5**, 380–385 (2002).

[19]C. R. Laing, "The dynamics of chimera states in heterogeneous Kuramoto networks," Physica D **238**, 1569–1588 (2009).

[20]O. E. Omel'chenko, "The mathematics behind chimera states," Nonlinearity **31**, R121–R164 (2018).

[21]E. A. Martens, C. R. Laing, and S. H. Strogatz, "Solvable model of spiral wave chimeras," Phys. Rev. Lett. **104**, 044101 (2010).

[22]S. Shima and Y. Kuramoto, "Rotating spiral waves with phase-randomized core in nonlocally coupled oscillators," Phys. Rev. E **69**, 036213 (2004).

[23]Y. Maistrenko, O. Sudakov, O. Osiv, and V. Maistrenko, "Chimera states in three dimensions," New Journal of Physics **17**, 073037 (2015).

[24]J. F. Totz, J. Rode, M. R. Tinsley, K. Showalter, and H. Engel, "Spiral wave chimera states in large populations of coupled chemical oscillators," Nature Physics **14**, 282–285 (2018).

[25]E. A. Martens, S. Thutupalli, A. Fourrire, and O. Hallatschek, "Chimera states in mechanical oscillator networks," Proceedings of the National Academy of Sciences **110**, 10563–10567 (2013).

[26]F. Parastesh, S. Jafari, H. Azarnoush, Z. Shahriari, Z. Wang, S. Boccaletti, and M. Perc,

"Chimeras," Physics Reports **898**, 1–114 (2021).

[27]S. W. Haugland, "The changing notion of chimera states, a critical review," Journal of Physics: Complexity **2**, 032001 (2021).

[28]I. Omelchenko, E. Omel'chenko, P. Hövel, and E. Schöll, "When nonlocal coupling between oscillators becomes stronger: patched synchrony or multichimera states," Physical review letters **110**, 224101 (2013).

[29]A. Vüllings, J. Hizanidis, I. Omelchenko, and P. Hövel, "Clustered chimera states in systems of type-i excitability," New Journal of Physics **16**, 123039 (2014).

[30]J. Hizanidis, V. G. Kanas, A. Bezerianos, and T. Bountis, "Chimera states in networks of nonlocally coupled hindmarsh–rose neuron models," International Journal of Bifurcation and Chaos **24**, 1450030 (2014).

[31]H. Sakaguchi, "Instability of synchronized motion in nonlocally coupled neural oscillators," Phys. Rev. E **73**, 031907 (2006).

[32]H. R. Wilson and J. D. Cowan, "A mathematical theory of the functional dynamics of cortical and thalamic nervous tissue," Kybernetik **13**, 55–80 (1973).

[33]C. R. Laing, "Dynamics and stability of chimera states in two coupled populations of oscillators," Physical Review E **100**, 042211 (2019).

[34]C. R. Laing, "Chimeras in networks of planar oscillators," Phys. Rev. E **81**, 066221 (2010).

[35]I. Omelchenko, A. Zakharova, P. Hövel, J. Siebert, and E. Schöll, "Nonlinearity of local dynamics promotes multi-chimeras," Chaos **25**, 083104 (2015).

[36]S. Olmi, "Chimera states in coupled kuramoto oscillators with inertia," Chaos **25**, 123125 (2015).

[37]D. Pazó and E. Montbrió, "Low-dimensional dynamics of populations of pulse-coupled oscillators," Physical Review X **4**, 011009 (2014).

[38]C. R. Laing, K. Rajendran, and I. G. Kevrekidis, "Chimeras in random non-complete networks of phase oscillators," Chaos **22**, 013132 (2012).

[39]I. V. Tyulkina, D. S. Goldobin, L. S. Klimenko, and A. Pikovsky, "Dynamics of noisy oscillator populations beyond the ott-antonsen ansatz," Physical review letters **120**, 264101 (2018).

[40]G. B. Ermentrout and N. Kopell, "Parabolic bursting in an excitable system coupled with a slow oscillation," SIAM Journal on Applied Mathematics **46**, 233–253 (1986).

[41]T. B. Luke, E. Barreto, and P. So, "Complete classification of the macroscopic behavior of a heterogeneous network of theta neurons," Neural computation **25**, 3207–3234 (2013).

[42]C. R. Laing, "Derivation of a neural field model from a network of theta neurons," Physical Review E **90**, 010901 (2014).

[43]C. R. Laing, "Exact neural fields incorporating gap junctions," SIAM Journal on Applied Dynamical Systems **14**, 1899–1929 (2015).

[44]C. R. Laing and O. Omel'chenko, "Moving bumps in theta neuron networks," Chaos **30**, 043117 (2020).

[45]E. Ott and T. M. Antonsen, "Low dimensional behavior of large systems of globally coupled

oscillators," Chaos **18**, 037113 (2008).

[46]E. Ott and T. M. Antonsen, "Long time evolution of phase oscillator systems," Chaos **19**, 023117 (2009).

[47]O. Omel'chenko, M. Wolfrum, and C. R. Laing, "Partially coherent twisted states in arrays of coupled phase oscillators," Chaos **24**, 023102 (2014).

[48]C. R. Laing, "Numerical bifurcation theory for high-dimensional neural models," The Journal of Mathematical Neuroscience **4**, 13 (2014).

[49]W. J. Govaerts, *Numerical methods for bifurcations of dynamical equilibria*, Vol. 66 (Siam, 2000).

[50]Y. Pomeau and P. Manneville, "Intermittent transition to turbulence in dissipative dynamical systems," Communications in Mathematical Physics **74**, 189–197 (1980).

[51]C. R. Laing, "Fronts and bumps in spatially extended kuramoto networks," Physica D **240**, 1960 – 1971 (2011).